Experimental Microbial Dysbiosis Does Not Promote Disease Progression in SIV-Infected Macaques

Alexandra M. Ortiz[1], **Jacob K. Flynn**[1], **Sarah R. DiNapoli**[1], **Ivan Vujkovic-Cvijin**[2], **Carly Elizabeth C. Starke**[1], **Stephen H. Lai**[1], **MacKenzie E. Long**[1], **Ornella Sortino**[1], **Carol L. Vinton**[1], **Joseph C. Mudd**[1], **Leslie Johnston**[3], **Kathleen Busman-Sahay**[3,4], **Yasmine Belkaid**[2,5], **Jacob D. Estes**[3,4,6], and **Jason M. Brenchley**[1,*]

[1]Barrier Immunity Section, Laboratory of Viral Diseases, National Institutes of Allery and Infectious Diseases (NIAID), National Institutes of Health (NIH), Bethesda, MD 20892, USA

[2]Mucosal Immunology Section, Laboratory of Parasitic Diseases, NIAID, NIH, Bethesda, MD 20892, USA

[3]AIDS and Cancer Virus Program, Frederick National Laboratory for Cancer Research, Leidos Biomedical Research, Inc., Frederick, MD, USA

[4]Vaccine and Gene Therapy Institute, Oregon Health and Science University, Beaverton, OR, 97006, USA

[5]NIAID Microbiome Program, NIH, Bethesda, MD, 20892, USA

[6]Oregon National Primate Research Center, Oregon Health and Science University, Beaverton, OR, 97006, USA

Abstract

Intestinal microbial dysbiosis has been described in HIV-1-infected individuals and may underlie persistent inflammation in chronic infection, thereby contributing to disease progression. Herein, we induced an HIV-1-like intestinal dysbiosis in rhesus macaques with vancomycin treatment and assessed the contribution of dysbiosis to SIV disease progression. Dysbiotic and control animals had similar disease progression, indicating that intestinal microbial dysbiosis similar to that observed in HIV-infected individuals is not sufficient to accelerate untreated lentiviral disease progression.

Intestinal microbial dysbiosis has been described in progressive HIV-1-infected individuals. This dysbiosis includes enrichment of Proteobacteria (particularly *Enterobacteriaceae*) and

Erysipelotrichaceae, coincident with declines in Clostridia and *Bacteroides*[1]. Dysbiotic taxa in infected individuals correlate with persistent inflammation – a hallmark of progressive infection[2]. However, an empirical assessment of the contribution of microbial dysbiosis to disease progression is lacking. Recent data suggest that risk factors for HIV-1 acquisition can also result in microbial dysbiosis[3] and although simian immunodeficiency virus (SIV) non-human primate (NHP) models for HIV-1 infection recapitulate salient features of infection[4], dysbiosis is not consistently observed[1,5].

In healthy NHPs, vancomycin inhibits the growth of Gram-positive bacteria, inducing a dysbiosis similar to that described in HIV-1 infection (Supplementary Fig. 1). To assess whether intestinal dysbiosis accelerates lentiviral disease progression, we treated 7 rhesus macaques (RMs) with vancomycin for 5 days, every 28 days, beginning 56 days pre-SIV infection (Fig. 1a) and infected these and 6 control animals with SIV$_{mac239}$. Following treatment, fecal microbiome diversity became increasingly disparate between groups, with vancomycin-treated (Vanco) animals exhibiting reduced α-diversity (taxa richness and evenness within a group) and increased β-diversity (phylogenetic distance of taxa between groups) compared to control animals (Fig. 1b and Supplementary Fig. 2a). No differences in total bacterial DNA recovery were observed between groups (Supplementary Fig. 2b).

Gram-positive Firmicutes dominated the fecal microbiome irrespective of treatment; however, relative Firmicute frequencies in Vanco animals decreased (Supplementary Fig. 2c). Whereas control animals had comparable distributions of Clostridia and Bacilli among Firmicutes, Firmicutes recovered from Vanco animals were enriched in Bacilli (Fig. 1c). Importantly, Vanco animals displayed increasing Proteobacteria frequencies post-infection (Supplementary Fig. 2c). Control animals had even distributions of Proteobacteria classes at d115 p.i., while Proteobacteria isolated from Vanco animals were enriched for Gammaproteobacteria (Fig. 1d). Epithelial-associated communities isolated from the large intestines of Vanco animals displayed similar enrichments for Proteobacteria relative to Firmicutes (Supplementary Fig. 2d).

Of 390 operational taxonomic units (OTUs) identified, 256 features were differentially present between control and Vanco animals at d115 p.i. as identified by LDA-effect size (LEFSE) algorithm (Fig. 1e, Supplementary Fig. 3, and Supplementary Dataset 1). The phylum Proteobacteria was enriched in Vanco animals and these enrichments were primarily driven by differences in Gammaproteobacteria (especially *Enterobacteriaceae*) and Deltaproteobacteria. In Vanco animals, LEFSE confirmed an enrichment of Bacilli and a depletion of Clostridia - particularly *Lachnospiraceae* and *Ruminococcaceae* - and *Erysipelotrichaceae* among Firmicutes while among Bacteroidetes, Bacteroidales and a sub-cluster of families were also moderately depleted. Principle coordinate analysis (PCoA) of identified OTUs at d115 p.i. revealed clustering of microbial communities by treatment (Fig. 1f). Longitudinal quantification of *Lachnospiraceae, Ruminococcaceae, Erysipelotrichaceae* and *Enterobacteriaceae* confirmed persistent alterations in Vanco animals (Supplementary Fig. 2e–f). Imputed metagenomic analysis revealed non-distinct fecal metagenomes between groups at baseline (Supplementary Fig. 4), with a notable enrichment for metabolic and virulence pathways in Vanco animals at d115 p.i. Short-chain fatty acids (SCFA) - microbial-produced metabolites important for GI immunity and epithelial barrier

maintenance[6,7] - were perturbed in Vanco animals, with significant disruptions from baseline observed for fecal valeric and hexanoic acids at d198 p.i. (Fig. 1g).

To assess interdependency of intestinal microbial dysbiosis and lentiviral disease progression, we first assessed the integrity of the intestinal epithelium. By immunohistochemical (IHC) staining for the tight junction protein Claudin-3, we observed reduced integrity of the colonic barrier in Vanco animals at necropsy (24.57% absence claudin-3 continuity in Vanco as compared to 6.602% in controls, 95% CI 10.18 – 25.75, p=0.0004; Fig. 2a). We next measured canonical parameters of disease progression. We found comparable: a) CD4+ T-cell counts and intestinal CD4+ T-cell frequencies (Fig. 2b and Supplementary Fig. 5a), b) plasma viral loads (Fig. 2c); c) memory CD4+ T-cell (TM)-associated viral DNA Fig. 2c and Supplementary Fig. 5b); and d) an equivalent depletion of intestinal CD4+ TM expressing the HIV/SIV co-receptor, CCR5 (Supplementary Fig. 5c), irrespective of treatment.

We next assessed whether intestinal microbial dysbiosis may impact immune activation by measuring phenotypic and functional markers of T-cells by flow cytometry. Between groups, isolated differences in cell-surface activation markers were observed in intestinal TM during acute infection (Supplementary Fig. 5c–d). Although stimulated jejunal CD8+ TM from Vanco animals displayed significant reductions in mitogen-induced IFNγ and TNFα at several timepoints (Supplementary Fig. 6a–c), these changes were not paired with differences in inhibitory PD-1[8] nor polyfunctionality[9] (Supplementary Fig. 6d–e), suggesting that intestinal microbial dysbiosis did not modulate immune activation.

To assess whether intestinal microbial dysbiosis increases microbial translocation, we measured *E. coli* in the colonic lamina propria, mesenteric lymph nodes (MLN), and livers of our animals by IHC and levels of plasma soluble CD14 (sCD14) and IL-6 by ELISA. Although both groups displayed evidence of translocation and elevated IL-6 (Fig. 2d–f), there were no differences. The Vancomycin-induced depletion of SCFA-producing commensal Clostridia - taxa important for induction and maintenance of antimicrobial lymphocytes - may predispose Vanco animals to the emergence of opportunistic infections by hindering the development or maintence[6] of IL-17-expressing CD4+ TM (T_H17), CD8+ TM (T_C17) and NKp44+ innate lymphoid cells type-3 (ILC3s)[5]. Despite differing Clostridia frequencies, we observed equivalent post-infection depletions of these subsets irrespective of treatment (Fig. 2f–g, Supplementary Fig. 6f) and a comparable presentation of secondary infections at necropsy (Supplementary Table 1).

In accordance with a lack of evidence for exacerbated immune dysfunction or microbial translocation, survival curves were comparable between groups, with control animals exhibiting a mean survival of 310 days p.i. and vancomycin-treated animals, 346 days p.i. (Fig. 2h; Mantel-Cox p=0.33, Hazard Ratio=0.6042 compared to control, 95% CI 0.192–1.902). Findings documented at necropsy included thrombosis, lymphadenopathy, and secondary infection (Supplementary Table 1); however, outcomes and blood cell counts (Supplementary Fig. 7) did not differ by group.

SIV-infection of RMs recapitulates key aspects of HIV-1 infection[4]. Although the gut microbial communities of RMs and humans share several dominant taxa, they differ substantially beyond the genus classification[10]. We cannot discount that underappreciated differences in viral, host, or commensal identity may uniquely contribute to lentiviral disease progression in human and NHPs; however, largely parallel disease progression between the two argues that shared mechanisms are responsible. Our data does not preclude a role for intestinal dysbiosis in lentiviral transmission[11], nor does it exclude a contribution of alternative dysbioses to lentiviral disease progression. Our data do, however, demonstrate that neither significant upheaval of the intestinal microbiome nor enrichment for Proteobacteria at the expense of Clostridia are sufficient for accelerating disease progression.

Conceivably, immune dysfunction resulting from viral replication may overshadow intestinal dysbiosis in HIV-infected individuals and microbial translocation may be saturated. Importantly, intestinal dysbiosis may contribute to inflammation observed in highly-active antiretroviral therapy (HAART)-treated individuals. This premise is supported by improved disease progression in HAART-treated RMs receiving additional microbiome-mediated therapeutics. Thus far, however, similar efficacy has not been achieved in placebo-controlled human trials. Whereas probiotic treatment in HIV-infected humans promotes modest decreases in T-cell activation and intestinal integrity, preliminary attempts towards fecal microbial transplantation have shown limited engraftment[12,13].

In conclusion, we demonstrate that experimentally-induced intestinal dysbiosis in SIV-infected RMs does not accelerate disease progression. Dysbiotic and control animals exhibited comparable viremia, target-cell depletion, immune activation, microbial translocation, and ultimately, survival rates. These data indicate that intestinal microbial dysbiosis similar to that observed in HIV-infected individuals is not sufficient to accelerate untreated disease progression. We do not know how or if vancomycin influenced the composition of the virome or mycobiome, both of which could influence inflammation[1,14]. Further studies are required to unravel the circumstances surrounding intestinal dysbiosis in HIV-infected patients and to determine whether components of specific dysbioses contribute to HIV transmission or therapeutic immune reconstitution.

ONLINE METHODS

Animals and Vancomycin Treatment

Thirteen healthy rhesus macaques (*Macaca mulatta*), aged 6–15, were assigned to a control (n=6, 5/6 male) or vancomycin treatment (n=7, all male) group, with sample size based on previous studies of experimental manipulations of disease progression in the macaque model. Groups were stratified by weight and genotype (Mamu-A*001, -A*002, -B*017, and -B*029) and animals sampled as mixed populations. Vancomycin-treated animals received vancomycin hydrochloride (Pfizer, 10 mg/kg, p.o.) for 5 days approximately every 28 days, beginning 56 days prior to infection. All animals were infected with 3000 $TCID_{50}$ SIV_{mac239} i.v. at d0 and were followed until clinical endpoints were met.

The NIAID Division of Intramural Research Animal Care and Use Program, as part of the NIH Intramural Research Program, approved all experimental procedures (protocol LVD 26). The Program complies with all applicable provisions of the Animal Welfare Act and other federal statutes and regulations relating to animals.

Animals were housed and cared for at the NIH Animal Center, under the supervision of the Association for the Assessment and Accreditation of Laboratory Animal Care (AAALAC)-accredited Division of Veterinary Resources and as recommended by the Office of Animal Care and Use Nonhuman Primate Management Plan. Husbandry and care met the standards set forth by the Animal Welfare Act, Animal Welfare Regulations, as well as The Guide for the Care and Use of Laboratory Animals (8th Edition). The physical conditions of the animals were monitored daily. Animals in this study were exempt from contact social housing due to scientific justification, per IACUC protocol, and were housed in non-contact, social housing where primary enclosures consisted of stainless steel primate caging. Animals were provided continuous access to water and offered commercial monkey biscuits twice daily as well as fresh produce, eggs and bread products twice weekly and a foraging mix consisting of raisins, nuts and rice thrice weekly. Enrichment to stimulate foraging and play activity was provided in the form of food puzzles, toys, cage furniture, and mirrors.

Sample Collection

Blood, tissue, stool and luminal swabs measurements are the result of a single sample per timepoint. Sampling occurred in the mornings and in random order, at predetermined timepoints as in Fig. 1A or upon meeting endpoint criteria as discussed below. Biopsies were maintained in RPMI before processing. For longitudinal LN biopsies, axillary or inguinal LNs were locally exposed and excised by blunt dissection. For longitudinal RBs, fecal material was removed from the rectum and biopsies obtained with biopsy forceps. Jej biopsies were obtained by video-guided endoscopy. Biopsies collected at necropsy were directly accessed immediately post-mortem. Stool was collected fresh from the colon of each animal and post-mortem luminal swabs were obtained by the swabbing of exposed luminal contents of intestinal tissues. Plasma was isolated from blood by centrifugation. Mononuclear cells were isolated from blood by Ficoll gradient centrifugation and from tissue biopsies by passing samples through a 0.22-μm cell strainer, with the exception of necropsy-obtained intestinal tissues. Endpoint jejunal and colonic biopsies (approximately 4 inches each) were mechanically and enzymatically digested in 120 mL of digestion media [RPMI supplemented to 10% fetal calf serum, 100 U/ml penicillin, 100 μg/ml streptomycin sulfate, 1.7 mM sodium glutamate, 0.1% Liberase™ (Sigma), and 1000U of DNAse I] for 1 hour at 37°C using a gentleMACS dissociator (Miltenyi) at 20 rpm, followed by treatment with 2mM dithiothreitol for 15 minutes at 37°C followed by 0.22-μm cell strainer filtration. Neither the investigators nor the animal handlers were blinded to group allocation in order to ensure multi-lateral supervision of design and palliative treatment. Animals were sedated with Ketamine HCL at 10 mg/kg i.m. for longitudinal blood sampling or with Telazol at 3–4 mg/kg i.m. for tissue timepoints. For jejunal biopsies, animals were further anesthetized with isoflurane gas by intubation, to effect. Successful anesthetization was monitored by response to stimuli.

Endpoint criteria included presentation of any of the following: (a) loss of 25% body weight from baseline weight when assigned to the protocol, (b) major organ failure or medical conditions unresponsive to treatment, (c) complete anorexia for 4 days or an inability to feed or drink sufficient nutrients to maintain body weight without assistance for 7 days, (d) distress vocalization unresponsive to treatment or intervention for 7 days, or (e) tumors arising from other than experimental means that grew in excess of 10% of body weight, impaired movement, or ulcerated. Euthanasia was initiated at clinical or experimental endpoints using protocols consistent with the American Veterinary Medical Association (AVMA) guidelines. Animals were first sedated with Telazol at 4 mg/kg i.m., followed by Pentobarbital at 80 mg/kg to achieve euthanasia.

Immune Phenotyping and Functional Assessment

Polychromatic flow cytometry and cell sorting were performed on stained mononuclear cells as previously described[15]. Antibodies against the following antigens were used for staining at predetermined concentrations: CD4 (clone OKT4), CD8 (SK1), IFNγ (4S.B3), IL-17 (eBio64DEC17), IL-21 (3A3-N2), IL-22 (IL22JOP), TNFα (MAb11), and PD-1 (J105) from eBioscience; CCR5 (3A9), CD3 (SP34-2), CD8 (SK1), CD16 (HI149), CD20 (2H7), CD23 (M-L233), CD45 (D058-1283), CD123 (7G3), and HLA-DR (L243) from BD; c-Kit (104D2), CD1a (HI149), CD11c (3.9), CD14 (M5E2), CD34 (561), CD95 (DX2), and IL-2 (MQ1-17H12) from Biolegend; CD127 (eBioRDR5) and CD218a (H44) from Thermo; NKp44 (2.9) from Miltenyi; and CD28 (CD28.2) from Beckman Coulter. CD4+ and CD8+ TM were defined as CD95+ singlet, clean, live, CD3+ lymphocytes. NKp44+ ILC3s were defined as CD45+ singlet, clean, live, lineage-negative (CD1a, CD3, CD8, CD11c, CD14, CD16, CD20, CD23, CD34, CD123), NKp44+CD127+CD218+ lymphocytes. Positive/ negative gating based on clearly grouped populations, historical-determined expression, and the use of internal controls (Supplementary Fig. 8). A threshold of 100 collected events in the parent population was utilized for all subset expression analysis.

16S isolation and analysis

DNA was isolated from 250 mg of stool using the PowerLyzer PowerSoil DNA isolation kit (MO BIO) substituting stool for soil during the initial processing steps. Samples were homogenized on a Precellys 24 (Bertin Technologies). The Biomek NK^P (Beckman Coulter) was used to facilitate automated, high-throughput processing via the PowerSoil manufacturer's protocol, substituting column binding with PowerMag magnetic beads and a magnetic plate (Alpaqua) on Corning 96 Deep-Well Assay Blocks (Fisher Scientific) to improve DNA retention throughout processing. 16S DNA was amplified from 50–100ng total DNA using barcoded universal primers spanning basepairs 515(F)-806(R) of the 16s rRNA V4 region. 16S amplicons were subjected to Agencourt AMPure XP PCR Purification (Beckman Coulter #A63882). >1ng 16S amplicons quantified using the 16S MiSeq (Illumina) platform. Returned FASTQ, paired-end reads were processed using QIIME[16] (v1.9.1) through the NIAID/NIH Microbiome Analysis Platform, Nephele (Office of Cyber Infrastructure and Computational Biology/NIAID/NIH. http://nephele.niaid.nih.gov), and reads were truncated before 3 consecutive bases having Phred quality scores below 20. OTUs were classified by open reference using SILVA_99, and data were rarefied at 1000 reads per sample. First-run, incomplete 16S miSeq timepoints were re-run in full with

banked stool and duplicate returns averaged per timepoint as listed in the NCBI Sequence Read Archive (SRA) under project number PRJNA417022. For metagenomic analysis, OTUs were reclassified by closed reference using Greenegenes_99, and metagenomic profiles predicted by PICRUSt[17]

Immunohistochemistry and quantitative image analysis

Formaldehyde fixed, paraffin-embedded (FFPE) tissue sections, 5μm thick, were placed on Fisher-Plus microscope slides, deparaffinized in xylenes, rehydrated through graded ethanols and subjected to HIER with 0.01% citraconic anhydride (Sigma-Aldrich; 125318), then cooled and washed in double distilled H_2O (ddH_2O), as previously described[18,19]. IHC for *E. coli* was performed on an intelliPATH autostainer (Biocare Medical): following incubation with blocking buffer (0.25% casein in tris-buffered saline (TBS) with 0.05% Tween-20) for 10 minutes and an endogenous peroxidase block of 1.5% (v/v) H_2O_2 in TBS (pH 7.4) for 10 minutes, slides were incubated with a rabbit polyclonal *E. coli* antibody (Dako, B0357; 3.8μg/ml) diluted in blocking buffer for 1 hour at room temperature and detected using a biotin-free anti-rabbit Polink-1 HRP polymer system (Golden Bridge International, Inc.) for 30 minutes at room temperature in conjunction with DAB (3,3′-diaminobenzidine; Vector Laboratories) for 2–5 minutes. IHC for claudin 3 was performed as above with the following modifications: slides were stained manually with a rabbit polyclonal claudin 3 antibody (Thermo Scientific, RB-9251-p; 1μg/ml) for 1 hour at room temperature. The slides were developed as described above. All slides were washed in ddH_2O, counterstained with hematoxylin, mounted with Permount (Fisher Scientific) and scanned at high magnification (×200) using a whole-slide scanning microscope (Aperio AT2 System, Aperio Technologies), yielding high-resolution data from the entire tissue section. For E. *coli* quantification, representative regions of interest (500×500 μm) were extracted from the whole-tissue scans and the percent area of the anatomical site of interest (lamina propria of the GI tract, T-cell zone of the LN) was quantified using Photoshop CS5 or CS6 (Adobe Systems, San Jose, CA) and Fovea (Reindeer Graphics, Asheville, NC) image analysis tools as previously described[18,19]. Claudin 3 staining was used to visualize epithelial tight junctions so as to quantify epithelial barrier integrity (percent damage) as previously described[18,19].

ELISAs

Concentrations of sCD14 and IL-6 were quantified from plasma using a commercially available ELISA kits (R&D DC140 and HS600B, respectively), according to the manufacturers' protocols.

SCFA

Fecal short-chain fatty acid concentrations were determined by gas chromatography (GC; Thermo Trace 1310 with TG-WAXMS A GC, 30 m, 0.32 mm, and 0.25 μm columns), by Creative Proteomics (division of Creative Dynamics; Shirley, NY). Fecal pellets were homogenized in 17% (w/w) water suspension, and titrated to pH 2.0 using 5M HCl. Fecal debris were pelleted and removed by centrifugation. The remaining supernatant was spiked with internal standard 2-Ethylbutyric acid. Samples were injected into the GC flame ionization detector and calibrated against a cocktail of standardized SCFAs – sodium

propionate and acetic, butyric, isobutyric, valeric, isovaleric, hexanoic, and heptanoic acids. Peaks were assigned using the Chromeleon 7.2 software (Thermo), based on retention times of individual SCFA components. Chromeleon automatically determined mM concentrations of sample peaks using peak integration.

VL and cell-associated viremia

Plasma viral RNA (vRNA) levels were determined by qRT-PCR (ABI Prism 7900 sequence detection system; Applied Biosystems). vRNA was reverse transcribed and cDNA amplified (45 cycles/default setting) with AmpliTaq Gold DNA polymerase (PCR core reagents kit; Perkin-Elmer/Roche) utilizing primer pairs corresponding to SIV_{mac239} gag gene sequences (forward, nucleotides 1181–1208, and reverse, 1338-1317). Cell-associated viral DNA within sorted CD4 TM cells was measured as previously[20]. Briefly, qRT-PCR was performed on sorted, lysed cells using the Taq DNA polymerase kit (Invitrogen) and the SIV_{mac239} forward primer GTCTGCGTCATYTGGTGCATTC, reverse primer CACTAGYTGTCTCTGCACTATRTGTTTTG, and probe sequence CTTCRTCAGTYTGTTTCACTTTCTCTTCTGCG.

Statistical Analyses

Statistical analyses of viremia, single parameter lymphocyte phenotype and function, and single microbial taxa frequency were performed using Prism (v7.0, GraphPad Software Inc.). Multiple t-tests (unpaired, two-way, with no correction for multiple tests or assumption of consistent standard deviations) were used for comparisons between groups; paired t-tests were used for intra-group comparisons. Averaged longitudinal data are presented as arithmetic mean ± standard error of the mean (SEM). Significance of polyfunctional cytokine expression was assessed using the Spice (v5.35; NIAID) permutation-test on relative expression values. Frequencies of microbial taxa are calculated relative to all returned bacterial OTUs mapping to non-mitochondrial (*Rickettsiales Mitochondria*) taxa. Microbial diversity was assessed by Chao1, Shannon, and unweighted and weighted Unifrac with statistical significance assessed by unpaired, two-way t-test for alpha indices and PERMANOVA (R-vegan function Adonis) for Unifrac distances. The empirical identification of differentially abundant bacterial taxa between groups was determined using the LEFSE algorithim[21] one-against-all multi-class analysis, normalized to 10^6 reads. PCoA plot of d115 p.i. Unweighted UNIFRAC distances generated by XLSTAT (Addinsoft v2017.5). PICRUSt-predicted metagenomic profiles were analyzed by STAMP[22], with significance assed by Welch's t-test with Storey's FDR (reported *$P<0.05$, effect size > 0.5). No data that met minimum threshold requirements as outlined in the Online Methods were excluded.

Data Availability

The 16S MiSeq data (Figs. 1–2 and Supplementary Fig. 1) were deposited in the NCBI SRA under project number PRJNA417022. Other data available from this study are available from the corresponding author upon reasonable request.

Supplementary Material

Refer to Web version on PubMed Central for supplementary material.

Acknowledgments

The content of this publication does not necessarily reflect the views or policies of DHHS, nor does the mention of trade names, commercial products, or organizations imply endorsement by the U.S. Government.

References

1. Ortiz AM, Brenchley JM. Curr Opin HIV AIDS. 2018; 13:15–21. [PubMed: 29028666]

2. Brenchley JM, Silvestri G, Douek DC. Immunity. 2010; 32:737–742. [PubMed: 20620940]

3. Noguera-Julian M, et al. EBioMedicine. 2016; 5:135–146. [PubMed: 27077120]

4. Policicchio BB, Pandrea I, Apetrei C. Front Immunol. 2016; 7:12. [PubMed: 26858716]

5. Mudd JC, Brenchley JM. J Infect Dis. 2016; 214(Suppl 2):S58–66. [PubMed: 27625432]

6. Ivanov II, et al. Cell. 2009; 139:485–498. [PubMed: 19836068]

7. Kelly CJ, et al. Cell Host Microbe. 2015; 17:662–671. [PubMed: 25865369]

8. Day CL, et al. Nature. 2006; 443:350–354. [PubMed: 16921384]

9. Betts MR, et al. Blood. 2006; 107:4781–4789. [PubMed: 16467198]

10. McKenna P, et al. PLoS Pathog. 2008; 4:e20. [PubMed: 18248093]

11. Gosmann C, et al. Immunity. 2017; 46:29–37. [PubMed: 28087240]

12. d'Ettorre G, et al. Immun Inflamm Dis. 2017; 5:244–260. [PubMed: 28474815]

13. Vujkovic-Cvijin I, et al. Gut Microbes. 2017; 0: [PubMed: 29087765]

14. Hager CL, Ghannoum MA. Curr Opin HIV AIDS. 2018; 13:69–72. [PubMed: 29028668]

15. Ortiz AM, et al. Mucosal Immunol. 2016; 9:458–467. [PubMed: 26286233]

16. Caporaso JG, et al. Nat Methods. 2010; 7:335–336. [PubMed: 20383131]

17. Langille MG, et al. Nat Biotechnol. 2013; 31:814–821. [PubMed: 23975157]

18. Estes JD, et al. PLoS Pathog. 2010; 6:e1001052. [PubMed: 20808901]

19. Hao XP, et al. Nat Commun. 2015; 6:8020. [PubMed: 26282376]

20. Brenchley JM, et al. Blood. 2012; 120:4172–4181. [PubMed: 22990012]

21. Segata N, et al. Genome Biol. 2011; 12:R60. [PubMed: 21702898]

22. Parks DH, et al. Bioinformatics. 2014; 30:3123–3124. [PubMed: 25061070]

Author Manuscript

Author Manuscript

Author Manuscript

Author Manuscript
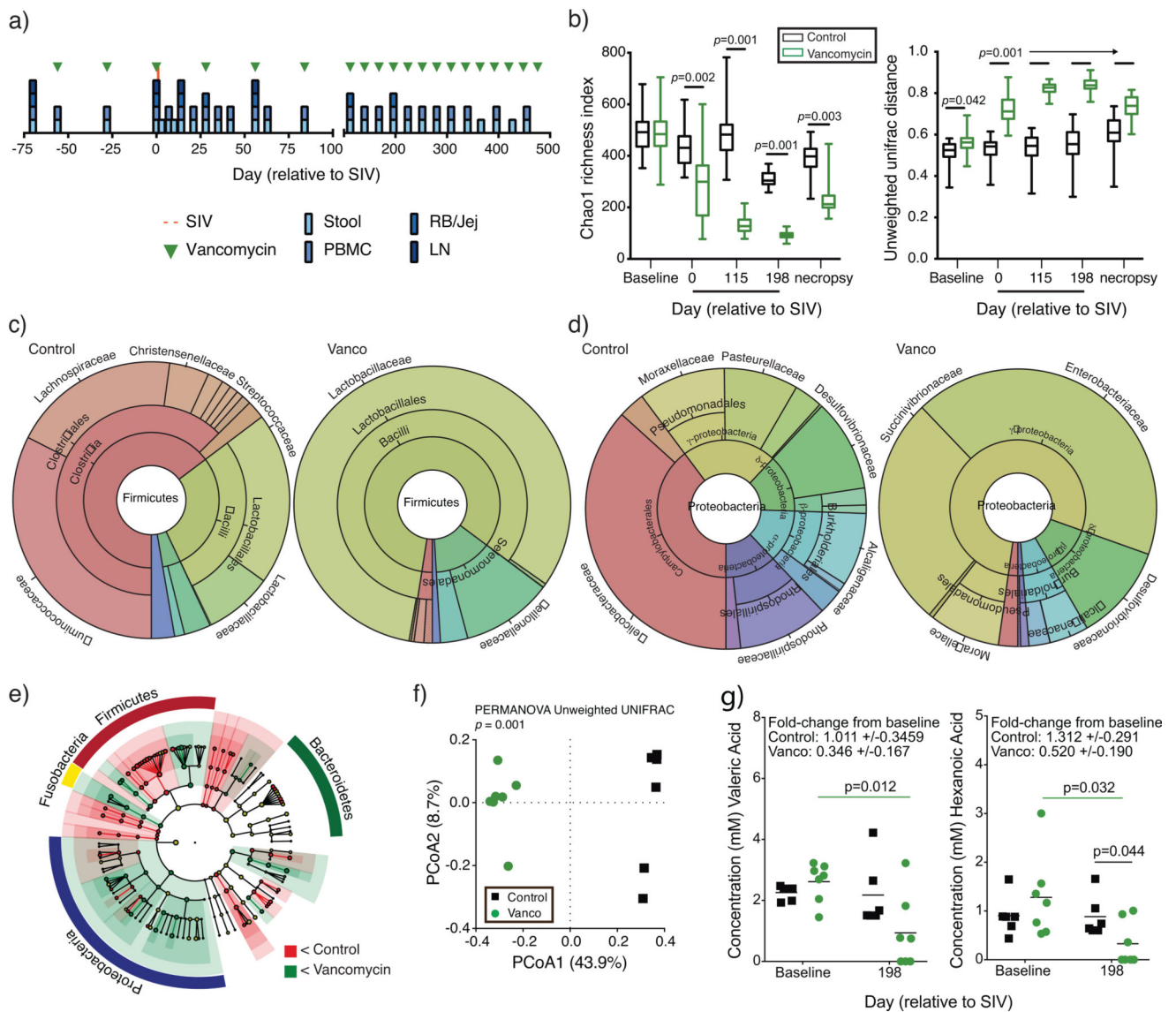
Figure 1. Vancomycin treatment promotes dysbiosis in SIV-infected RMs

(a) Longitudinal study design depicting timepoints for vancomycin treatment, SIV-infection, and specimen sampling. (b) Diversity measures Chao1 (α-diversity; left) and unweighted Unifrac (β-diversity; right) of fecal microbiome in RMs at indicated timepoints. Hinges span 25th–75th percentiles, center denotes mean, and whiskers represent min-to-max values. (c) Krona plots depicting relative frequency of fecal Firmicute subtaxa comprising ≥ 5% phylum burden at d115 p.i. to the family level. Shown taxa are collapsed to the lowest common taxon. (d) Krona plots depicting relative frequency of Proteobacteria as in c. (e) Cladogram depicting significantly disparate fecal taxa frequencies at d115 p.i. to the level of family where nodes and overlays in red highlight features enriched in control animals and those in green, Vanco animals. Arcs demarcate phyla of interest. (f) PCoA of Unweighted UNIFRAC distances measured at d115 p.i. (g) Fecal short-chain fatty acids at baseline and d198 p.i. Average line represents mean. *p*-values for comparison between timepoints span timepoints; those for inter-group analysis span compared groups. d198 p.i. mean fold-change +/−SEM

from baseline values denoted on graphs. For all timepoints, samples were obtained from n=6 and 7 longitudinally accessed control and vancomycin-treated animals respectively, except for d-56 (n=5 and 7) and d198 (n=6 and 6) in **b–f**. Sequence reads per animal are an average of 1–2 reads per timepoint as listed in the NCBI SRA (PRJNA417022). Alpha diversity indices represent the mean of 10 iterations of 1000 sequences per sample. Statistical significance of vancomycin effect on α-diversity in **b** and for inter-group analysis in **g** determined by unpaired, two-way t-test. Intra-group analysis in **g** by paired, two-way t-test. Significance of vancomycin effect on fecal β-diversity in **b** and **f** assessed by PERMANOVA. Significantly enriched features highlighted in **e** were identified by LEFSE.
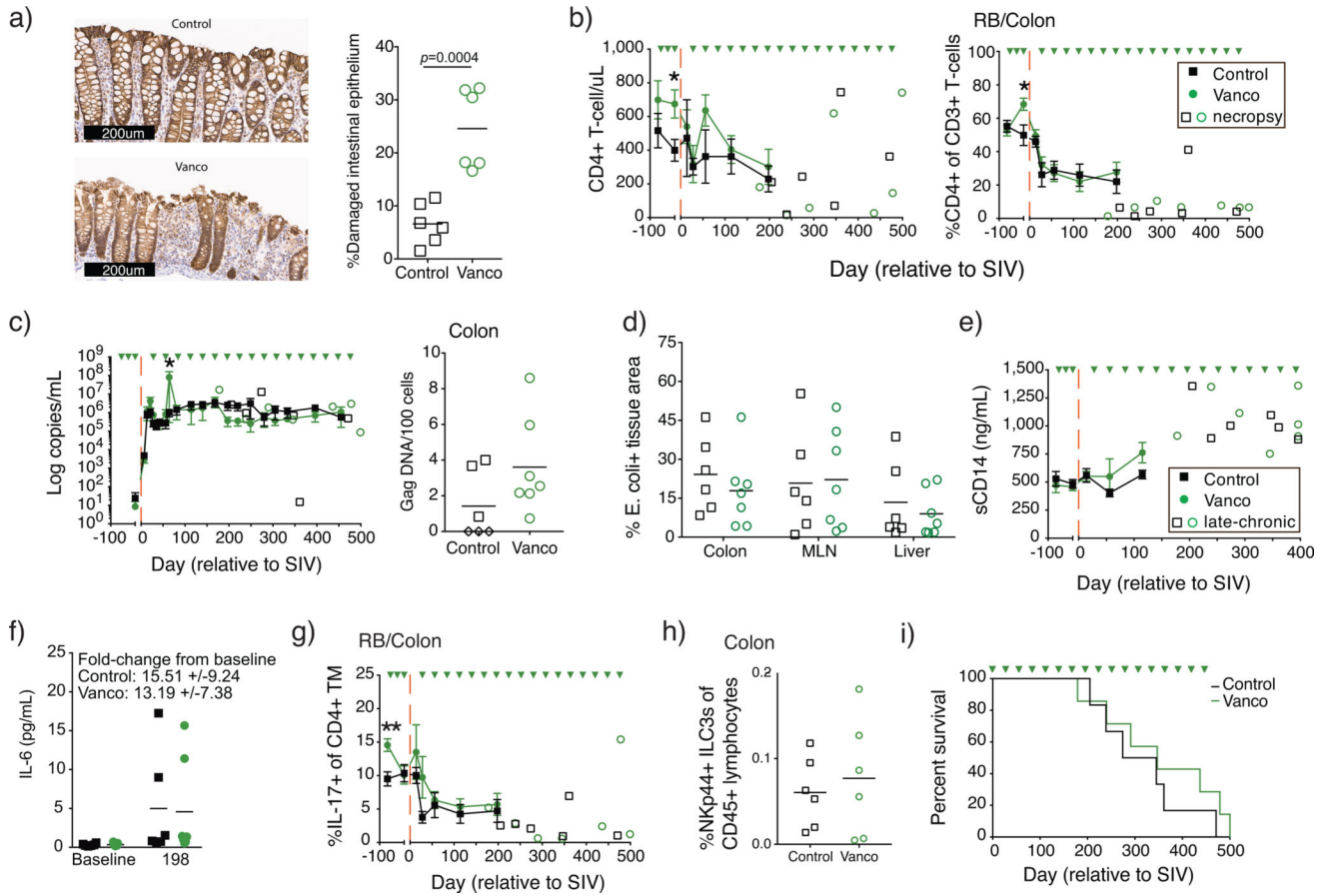
Figure 2. SIV disease progression is unaffected by vancomycin-induced intestinal dysbiosis
(a) IHC Claudin-3 staining in representative colon sections (left) and as mean percent negative epithelial perimeter (epithelial damage; right) at necropsy. **(b)** Mean, longitudinal circulating CD4+ T-cell counts (left) and RB/Colon CD4+ TM frequencies (right). *denotes p-value between groups at d0 of 0.028 for CD4+ T-cell count and 0.021 for RB %CD4+ T-cells. **(c)** Mean, longitudinal plasma viral loads (left) and cell-associated viral loads from Colon CD4+ TM at necropsy (right). Samples below the limit of detection reported as open diamonds. *denotes p=0.042 at d28 **(d)** Mean percent IHC positive *E. Coli* tissue area from necropsy Colon (lamina propria), MLN, and liver. **(e)** Mean, longitudinal, circulating sCD14 concentrations. **(f)** Individual plasma IL-6 concentrations at Baseline and d198 p.i. Average line represents mean. d198 p.i. mean fold-change +/−SEM from baseline values denoted on graphs **(g)** Mean, longitudinal frequencies of RB/Colon T_H17. **denotes p=0.005 between groups at baseline. **(h)** Mean frequency of Colon NKp44+ ILC3 at necropsy. **(i)** Survival curve depicting time to death. Samples were longitudinally accessed from n=6 and 7 for control and vancomycin-treated animals respectively, except for: d198 (n=6 and 6); in **c**, where timepoints d198p.i. depict mean viremia for all surviving animals; in **g**, at d-68 and d14 (n=6 and 6), d0 (n=5 and 6), d28 (n=3 and 4), and d115 (n=5 and 7); and in **h** (n=6 and 6). Longitudinal lines represent mean and include ±SEM where individual data points are

not shown. Statistical significance between groups assessed by unpaired, two-way t-test. Survival significance in **i** was assessed by Mantel-Cox.